Screened real-space Korringa-Kohn-Rostoker description of the relativistic and magnetic properties of transition metals

2000 J. Phys.: Condens. Matter 12 8439

(http://iopscience.iop.org/0953-8984/12/39/307)

J. Phys.: Condens. Matter **12** (2000) 8439–8454. Printed in the UK PII: S0953-8984(00)14811-8

Screened real-space Korringa–Kohn–Rostoker description of the relativistic and magnetic properties of transition metals

L Petit†‡, S V Beiden†, W M Temmerman§, Z Szotek§, G M Stocks‖ and G A Gehring†

† Department of Physics and Astronomy, University of Sheffield, Sheffield S3 7RH, UK
‡ Institut de Physique et de Chimie des Matériaux de Strasbourg, 28 rue du Loess, 67037 Strasbourg Cédex, France
§ Daresbury Laboratory, Daresbury, Warrington WA4 4AD, UK
‖ Oak Ridge National Laboratory, Oak Ridge, TN 37831, USA

Received 19 June 2000, in final form 4 August 2000

Abstract. The use of the relativistic and spin-polarized real-space Korringa–Kohn–Rostoker (KKR) method is limited to small systems (less than 100 atoms). This is due to the prohibitively large CPU times needed for the inversion of the KKR matrix. To study systems of more than a thousand atoms, we have implemented the concept of a screened reference medium, within the fully relativistic spin-polarized version of the real-space locally self-consistent multiple-scattering method (LSMS). The LSMS method makes use of a local interaction zone (LIZ) for solving the quantum mechanical problem, while the Poisson equation is solved in the whole space. The screened reference medium gives rise to sparse KKR matrices and using state-of-the-art sparse matrix technology a substantial reduction in the CPU times is obtained, enabling applications of the method to systems whose LIZ consists of more than a thousand atoms. The method is benchmarked by application to the elemental transition metals, the fcc (face-centred-cubic) Co and Ni, and the bcc (body-centred cubic) Fe, and compared to the results of the conventional $\boldsymbol{k}$-space methods. The convergence in real space of the magnetic moments, the magnetocrystalline anisotropy energy and the orbital moment anisotropy is discussed in detail.

1. Introduction

First-principles quantum mechanical calculations of the magnetic properties of periodic solids are usually performed by means of $\boldsymbol{k}$-space methods. However, not for all problems of interest can one exploit translational invariance. These include compositional inhomogeneities and strains at surfaces, interfaces and grain boundaries, nanostructures such as nanowires and nanoclusters with potential applications as giant-magnetoresistance (GMR) systems [1, 2]. Very often, the lowering or loss of symmetry determines the technological importance of materials. The magnetocrystalline anisotropy energy (MAE), for example, tends to be much larger at the surface than in the bulk, and its direction in thin films is determined by the deposited material and the layer thickness [3, 4].

In $\boldsymbol{k}$-space, surfaces can be treated as layered structures with the two-dimensional periodicity in the plane, and one real-space dimension in the perpendicular direction. If planar disorder occurs, one uses large two-dimensional unit cells, which are periodically repeated. Inside these cells, the real-space problem has to be addressed. At interfaces and grain boundaries, the periodicity is eventually completely lost and the problem needs to be treated entirely in real space.

0953-8984/00/398439+16$30.00

In this paper, we present the screened real-space fully relativistic spin-polarized Korringa–Kohn–Rostoker (KKR) method. Here real space is implemented along the lines of the locally self-consistent multiple-scattering (LSMS) formalism [5, 6], where it is assumed, for each site of the solid, that the quantum mechanics is determined by the surrounding atoms, while the Poisson equation is solved in the whole space. Thus, each site is considered as the centre of a local interaction zone (LIZ), and the electron density on this site is calculated by considering only the multiple-scattering processes from the neighbouring sites in the LIZ.

Incorporating relativistic effects in the unscreened version of the LSMS method, Beiden *et al* [7, 8] have explored the convergence, as a function of the LIZ's size, of the spin and orbital magnetic moments and the magnetocrystalline anisotropy energy of elemental transition metals. Fast convergence in real space has been observed for the bcc Fe and the fcc Co. For the fcc Ni, for less than four shells of atoms in the LIZ, no magnetic moment has been obtained. Moreover, no convergence for the magnetic moment and the MAE has been observed within the LIZs of up to 135 atoms (seven shells).

In the unscreened formalism, it is very difficult to deal with the LIZs of more than a hundred atoms, because the inversion of the KKR matrices scales as $O((2 \times (l_{max} + 1)^2 \times M)^3)$ with the number M of atoms in the LIZ. Here l_{max} defines the angular momentum cut-off, and the overall multiplication by 2 is due to the relativistic quantum mechanics. The required CPU times become quickly prohibitive. However, on introducing the screened reference medium [9], a concept originating from Andersen's tight-binding formalism [10, 11], and implemented in the KKR method by Zeller *et al* [12], the structure constant matrices become sparse and, as has been previously shown [13], the matrix inversion times can be substantially reduced by using state-of-the-art sparse matrix technology. Consequently, as will be demonstrated in the present paper, much larger LIZs become accessible to numerical investigation.

The screening technique has so far been applied to situations where real space enters either as zero or one dimension. It is either used as a means to generate $\boldsymbol{k}$-dependent structure constants by a lattice Fourier transform, without the need to use the Ewald summation [14], or in applications to layered systems where a two-dimensional Fourier transform over the layer is performed whilst the remaining dimension is dealt with in real space [16]. Here we present a study with screening without any lattice Fourier transform. Such a study has not been done before and the motivation was to determine the convergence of the method and the usefulness of this approach for calculating the magnetocrystalline anisotropy energy for complex systems. An important aspect of our approach is the use of state-of-the-art sparse matrix technology [17] to push our method to the largest possible system sizes with the present generation of workstations. The physics being targeted by this methodology is the study of the MAE and the orbital moment anisotropy in circumstances of low symmetry which occur at relaxed surfaces and interfaces, steps at surfaces, impurities and surface alloying. These are situations that cannot easily be studied by $\boldsymbol{k}$-space methods.

The remainder of the paper is organized as follows. In the next section, we present the formalism of the screened real-space KKR method, and discuss difficulties associated with the non-periodic reference medium. In section 3, we describe how to construct the screened structure constant matrix, and introduce the approximations enabling us to study systems with significantly more than a thousand atoms. Here, to benchmark the present method against the existing $\boldsymbol{k}$-space methods, all calculations have been performed for the elemental fcc Co and Ni, and the elemental bcc Fe. In section 4, we concentrate on the convergence of the magnetic moments, and discuss the validity and accuracy of the approximations employed. We compare the present results for the spin and orbital moments, and the MAE and the orbital moment anisotropy (OMA), for Fe, Co and Ni, to those obtained with the standard $\boldsymbol{k}$-space methods. Finally, in section 5, we draw our conclusions.

2. Theory

For the sake of clarity and comparison with the $\boldsymbol{k}$-space methods, in this paper we concentrate on bulk materials, with all atoms equivalent. In the LSMS formalism such systems are approximated by a single LIZ consisting of M atoms of the material: LIZ $= \{p\}$ where the sites p are such that $|\boldsymbol{R}_p - \boldsymbol{R}_0| < \boldsymbol{R}_{LIZ}$, i.e. the atoms are contained within a sphere of radius $\boldsymbol{R}_{LIZ}$ around the central site $\boldsymbol{R}_0$. Beyond the $\boldsymbol{R}_{LIZ}$, the boundary of the LIZ, the potential is set to zero, i.e. the muffin-tin zero. The Poisson equation is solved for the infinite real system, whereas for the quantum mechanical problem the LIZ is used. The scattering-path matrix for the cluster of M atoms is obtained as

$$\tilde{\tau}_M(E) = [\tilde{t}_M^{-1}(E) - \tilde{G}_M^0]^{-1}. \tag{1}$$

The LIZ t-matrix, $\tilde{t}_M$, has M non-zero sub-blocks on the diagonal, each corresponding to a specific single-site scattering matrix t_j, where j is one of the M atoms in the local interaction zone. The free-space structure constant matrix, $\tilde{G}^0$, consists of the site- and angular-momentum-decomposed matrix elements of the free-space propagator:

$$\tilde{G}_M^0 = \{\tilde{G}^{0;pn}(E)\} \qquad \tilde{G}^{0;pn}(E) = \{G_{LL'}^{0;pn}(E)\} \tag{2}$$

where p and n run over all the sites in the LIZ.

The electronic and magnetic properties are derived from the multiple-scattering Green's function, $G(\boldsymbol{r}, \boldsymbol{r}'; E)$, of the system. In the vicinity of the central site $\boldsymbol{R}_0$, it can be written as [18, 19]

$$G(\boldsymbol{r}, \boldsymbol{r}'; E) = \sum_{\Lambda,\Lambda'} Z_\Lambda(\boldsymbol{r}_0)\tau_{\Lambda\Lambda'}^{00}(E)Z_{\Lambda'}^\times(\boldsymbol{r}_0') - \sum_\Lambda Z_\Lambda(\boldsymbol{r}_<)J_\Lambda^\times(\boldsymbol{r}_>). \tag{3}$$

Here, $\boldsymbol{r}_0 = \boldsymbol{r} - \boldsymbol{R}_0$ and $\boldsymbol{r}_0' = \boldsymbol{r}' - \boldsymbol{R}_0$, and $\boldsymbol{r}_<$ ($\boldsymbol{r}_>$) means the smaller (bigger) of $(\boldsymbol{r}, \boldsymbol{r}')$. The relativistic Green's function, $G(\boldsymbol{r}, \boldsymbol{r}'; E)$, is a 4×4 matrix, Λ stands for the pair of relativistic quantum numbers (κ, μ), and Z_Λ and J_Λ represent respectively the normalized regular and irregular scattering solutions to the single-site Dirac equation. $\times$ refers to taking the complex conjugate of only the spherical harmonic, and not the radial part of these solutions. The site-diagonal matrix elements of the scattering-path operator, $\tau_{\Lambda,\Lambda'}^{00}$, give the scattered wave at site 0, due to an incident wave at 0, taking into account all possible scattering processes in between. It is obtained as the 00 site-diagonal sub-block of $\tilde{\tau}_M$ of equation (1) and is actually the only part of $\tilde{\tau}_M$ which is needed for the Green's function of equation (3).

In the KKR method, knowledge of the Green's function, $G(\boldsymbol{r}, \boldsymbol{r}'; E)$, allows one to calculate such quantities as the charge density $\rho(\boldsymbol{r})$, spin magnetic moment $\boldsymbol{m}_{spin}$ and orbital magnetic moment $\boldsymbol{m}_{orb}$.

The force theorem [20], which follows from the variational character of the total energy, defines the change in the total energy between two states with similar charge densities to be equal to the change in the sum of the one-electron energies E_{sum}. Consequently, the magnetocrystalline anisotropy energy, being the difference in the total energies corresponding to two different magnetization directions, is defined as

$$E_{MCA} = \sum_i^{occ} E_i^{[\hat{M}_1]} - \sum_i^{occ} E_i^{[\hat{M}_2]} = \int^{E_{F_1}} \mathrm{d}E\, n_{[\hat{M}_1]}(E)E - \int^{E_{F_2}} \mathrm{d}E\, n_{[\hat{M}_2]}(E)E \tag{4}$$

where $n_{[\hat{M}_1]}(E)$ and $n_{[\hat{M}_2]}(E)$ are the single-particle densities of states when the magnetization is in the directions $[\hat{M}_1]$ and $[\hat{M}_2]$, respectively. Here E_{F_1} and E_{F_2} are the Fermi energies corresponding to the single-particle densities of states $n_{[\hat{M}_1]}(E)$ and $n_{[\hat{M}_2]}(E)$.

The major computational effort of the real-space method is associated with the determination of $\tau_{\Lambda,\Lambda'}^{00}$ through the matrix inversion in equation (1). The free-space structure

constants are long ranged, i.e., all the sites in the LIZ are connected to all the other sites in the LIZ, and the matrix inversion times scale as $O(N^3)$ with the matrix dimension N. Following Andersen *et al* [10, 11], Zeller *et al* [12] have proposed a new reference medium where the structure constants decay exponentially in real space. This reference medium consists of spherically symmetric constant repulsive potentials at the non-overlapping muffin-tin sites. In the interstitial space, the potential remains zero. The exponential decay of the corresponding so-called 'screened' structure constants is due to the fact that, in the energy range of the valence bands, and with repulsive potentials in excess of 2 Ryd, there exist no eigensolutions for the new reference system.

The scattering with respect to the new reference medium is described by the scattering matrix

$$\Delta t_j = t_j - t_j^{sc} \tag{5}$$

where t_j and t_j^{sc} are respectively the t-matrices of the muffin-tin potential and the repulsive potential. The structural Green's function for the screened reference medium is obtained from the Dyson equation

$$\tilde{G}_M^{sc} = \tilde{G}_M^0(\tilde{I} - \tilde{t}_M^{sc}\tilde{G}_M^0)^{-1}. \tag{6}$$

Similarly to equation (3), the Green's function for the LIZ can be written in terms of the new scattering-path operator:

$$\tilde{\tau}_{\Delta,M}(E) = [(\Delta\tilde{t})_M^{-1}(E) - \tilde{G}_M^{sc}]^{-1} \tag{7}$$

and the single-site solutions are now defined with respect to the difference scattering potential.

The change of reference medium is a purely mathematical concept, and completely identical Green's functions are obtained when the matrices in equation (6) involve the entire LIZ. However, it has been shown by Zeller [14] that, because of the exponential decay in real space, the screened structure constants connecting sites at $\boldsymbol{R}_n$ and $\boldsymbol{R}_p$, can be ignored if $|\boldsymbol{R}_n - \boldsymbol{R}_p| > R_{sc}$, and that only those with $|\boldsymbol{R}_n - \boldsymbol{R}_p| < R_{sc}$ need be considered. Here R_{sc} denotes a certain distance, called the screening radius, beyond which the screened structure constants are essentially zero. Consequently, the screened structure constants are still calculated through the Dyson equation (6), but by inverting clusters of much smaller size than the LIZ.

In periodic systems, all the sites of the infinite reference medium are equivalent, and the $\boldsymbol{k}$-space screened structure constants, $G_{LL'}^{sc}(\boldsymbol{k}, E)$, can be calculated by lattice Fourier transformation. Because of the exponential decay, the summation converges fast and does not require the Ewald procedure [14]. When applied to layered systems, the screening leads to band diagonal matrices [15, 16]. In real space, the important feature associated with the new reference medium is the sparsity of the screened structure constants, which results from the exponential decay of its matrix elements in real space. In fact, as has been shown in reference [13], by applying a specific sparse matrix solver [17], and depending on the degree of sparsity, the inversion scales essentially as $O(N)$ with matrix dimension N. This means that we can expect considerable gains in the execution times of our code when exploiting the freedom of choice of the reference medium.

There is however a drawback. The structure constants for the free-space reference medium are known analytically, whereas the screened structure constants have to be calculated numerically (equation (6)). As can be seen from figure 1, our reference system for the LIZ is not translationally invariant. The repulsive potentials are placed only on those sites that correspond to atoms in the LIZ. Outside this zone, the reference medium is the free space. Therefore, every site is surrounded by a different scattering neighbourhood, and the screened structure constant matrix for the LIZ cannot be reconstructed by translations of the screened

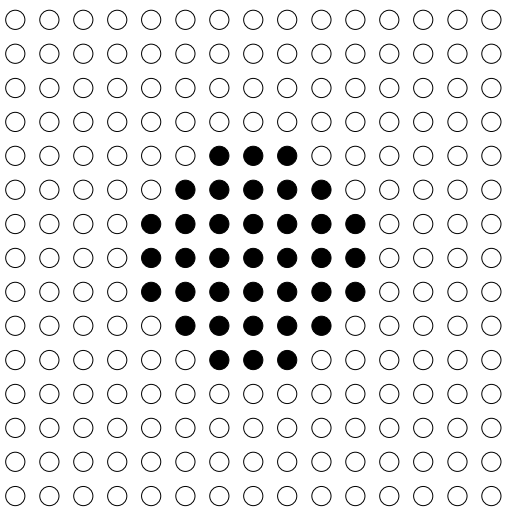

Figure 1. The reference medium for the screened real-space method. In the area covered by the LIZ, constant repulsive potentials at the muffin-tin sites are used (dark spheres). Outside this area the reference medium is free space (white spheres).

structure constants, calculated for one limited small cluster contained within a screening radius. To find the screened structure constant matrix we can either invert the matrix for the entire LIZ, which is clearly not an economical solution, or we can calculate the screened structure constants for each site of the LIZ by inverting a small matrix corresponding to the sites within its screening radius. This means that some of the gain in CPU time that results from dealing with sparse matrices will be lost in the construction of these matrices.

The speeding up in the matrix inversions, with respect to ordinary LU decomposition, allows one to study much larger cluster sizes than was previously possible. In the next section we will discuss how this gain in the CPU time can be maximized, and what approximations can be used to further increase the size of the LIZs.

3. Matrix construction and approximations

The execution time of the sparse matrix inversion is to a large extent determined by the degree of sparsity, i.e., the number of matrix elements that are zero. Therefore, the aim is to make the screened structure constants as short ranged as possible. However, a cutting off of the screened structure constants after only a few shells, for example a screening radius of one or two shells, can only be justified if the height of the repulsive potentials causes the screened structure constants to decay quickly enough that they can be neglected beyond that distance. Moreover, the height of the repulsive potentials has to be chosen according to the energy window of applicability. It has been previously noted [14] that the energy range of applicability of the screened KKR method is larger for higher potentials, and that accurate densities of states (DOS) for energies of up to 3 Ryd can be obtained with a repulsive potential of 8 Ryd. In the present work we have used a screening potential of 4 Ryd to reproduce reliably the DOS at the energies corresponding to the valence bands and the angular momenta up to $l_{max} = 3$.

Concerning the screening radius, we find that three shells of screening are sufficient to reproduce the DOS of bcc Fe. For Co and Ni, which crystallize in the more close packed fcc structure, two shells of screening are sufficient. Compared to the unscreened results, for these

respective screening radii, the total energies are reproduced with the precision of 10^{-3} Ryd, whereas the spin magnetic moments have been calculated with the accuracy of 10^{-1} μ_B. A larger screening radius implies more accurate computed values, meaning that for example the spin magnetic moment of Fe can be determined with the accuracy of 10^{-3} μ_B, when a screening radius of five shells is used. However, in this case, the sparsity of the screened structure constant matrix is considerably reduced, and the matrix inversion time increases accordingly.

In the absence of structural disorder in the cluster, in the central region of the cluster the translational invariance is fulfilled, and only the sites at the surface are surrounded by a different number of sites within the screening radius. Moving to ever-increasing cluster sizes, the relative importance of the surface with respect to the central area decreases. Therefore, one might expect that for large LIZs, it would be a good approximation to assume translationally invariant structure constants on all the sites. We have tested this assumption by calculating the spin magnetic moment on the central site of the Co cluster as a function of the number of shells in the LIZ. As can be seen in figure 2, even with 29 shells (1055 atoms) in the LIZ, the magnetic moment shows no sign of convergence. Since, however, it has been shown in the unscreened calculations [7] that the magnetic moment has been converged for smaller LIZs, we have to conclude that the use of the translationally invariant screened structure constants is not justified. Assuming translationally invariant screened structure constants is equivalent to having a reference medium with the repulsive potentials both inside and outside the LIZ. The physical picture that it corresponds to is that of a muffin-tin potential within the LIZ, embedded in a repulsive potential, giving rise to a quantum well with standing waves inside the chosen cluster [21]. In calculations for layered systems, with only one real-space dimension, this problem, though noticeable, is less serious [16].

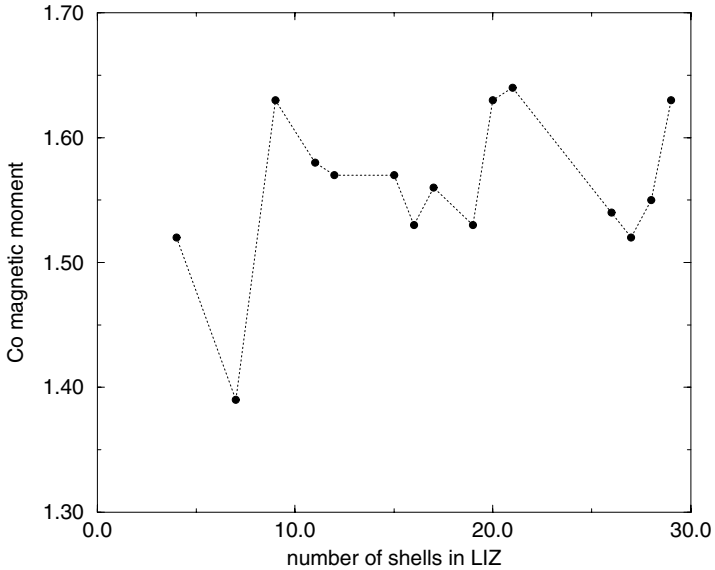

Figure 2. The magnetic moment of Co as a function of the number of shells in the LIZ. The reference medium is assumed to be translationally invariant.

The matrix dimension N is determined by the size of the LIZ, and the angular momentum expansion of the structure constants, i.e., $N = 2(l_{max} + 1)^2 \times M$, where l_{max} is a maximum value of the on-site angular momentum cut-off. It has been suggested earlier [7] that it is

sufficient to use large values for l_{max} only on the first few shells of the cluster, and to reduce l_{max} on more distant shells of the LIZ cluster. This of course reduces the matrix dimension considerably, as we now have

$$N = \sum_{i=1}^{M} 2(l_{max,i} + 1)^2$$

with i the atom index for the M-atom LIZ. In a tight-binding picture of the electronic structure, this approximation can be justified by noting the fact that for example the d electrons are more localized than the s electrons, and therefore the d levels on a remote atom will only have a negligible effect on the electronic properties of the central site. If this approximation were justified, it would be sufficient to use only $l_{max} = 0$ on all the outer sites of the cluster. This would imply further that one could consider extremely large LIZ sizes, and at the same time reduce the time needed for the reconstruction of the screened structure constant matrix. We shall explore this possibility further in the next section.

4. Results and discussion

In comparison with the standard KKR $\boldsymbol{k}$-space calculations, the present method relies on three major approximations: the size of the LIZ, the angular momentum cut-off and the screening radius. In this section we shall discuss our results for the convergence of the magnetic properties on the central site of the LIZ as a function of the number of shells in the LIZ. Furthermore, we shall analyse the dependence of the results on the angular momentum cut-off, i.e., the second approximation. The third approximation, associated with the value of the screening radius, is considered when comparing our results to those of the equivalent $\boldsymbol{k}$-space methods.

4.1. Convergence

In figure 3 we show the convergence of the spin and orbital magnetic moments in Co, as a function of the number of shells in the LIZ. The angular momentum configuration in the LIZ used in these calculations is referred to as $l_{max} = 3^3 2^6 1^n$, meaning that on the central site and the nearest- and second-nearest-neighbour shells we have included angular momenta up to $l_{max} = 3$, then on the atoms belonging to the six subsequent shells we have set $l_{max} = 2$ and for the rest of the sites we have used $l_{max} = 1$. For Fe, shown in figure 4, additionally to the angular configuration used for Co, we have also performed calculations for the $l_{max} = 3^3 2^m$ configuration and the corresponding results are plotted in the relevant panel for comparison. As can be seen in figure 5, the latter configuration has also been studied for Ni, but instead of the $l_{max} = 3^3 2^6 1^n$ angular momentum configuration, we have performed calculations for the $l_{max} = 3^3 2^6 0^n$ configuration. Our test studies have shown that, although the converged value depends on the choice of the screening radius, the convergence pattern is independent of it. As a consequence, the observed convergence behaviour has been obtained by using screening radii of respectively one shell for Co and Ni, and two shells for Fe.

As can be seen in figure 3, in the case of Co for LIZs larger than 17 shells, i.e., 459 atoms, all the calculated properties for the central site are converged. The magnetic moments of Fe are seen to converge at around 17 shells in the LIZ. The converged value is 2.05 μ_B. This value differs by approximately 0.05 μ_B from the result obtained with three shells of screening, i.e., a change of 2.5%. The results obtained with three shells of screening are generally in better agreement with the results obtained with the free-space reference medium.

For Ni the situation is different. It has been noticed in the unscreened calculations that one has to include at least five shells in the LIZ to obtain a magnetic moment at all [7], and that

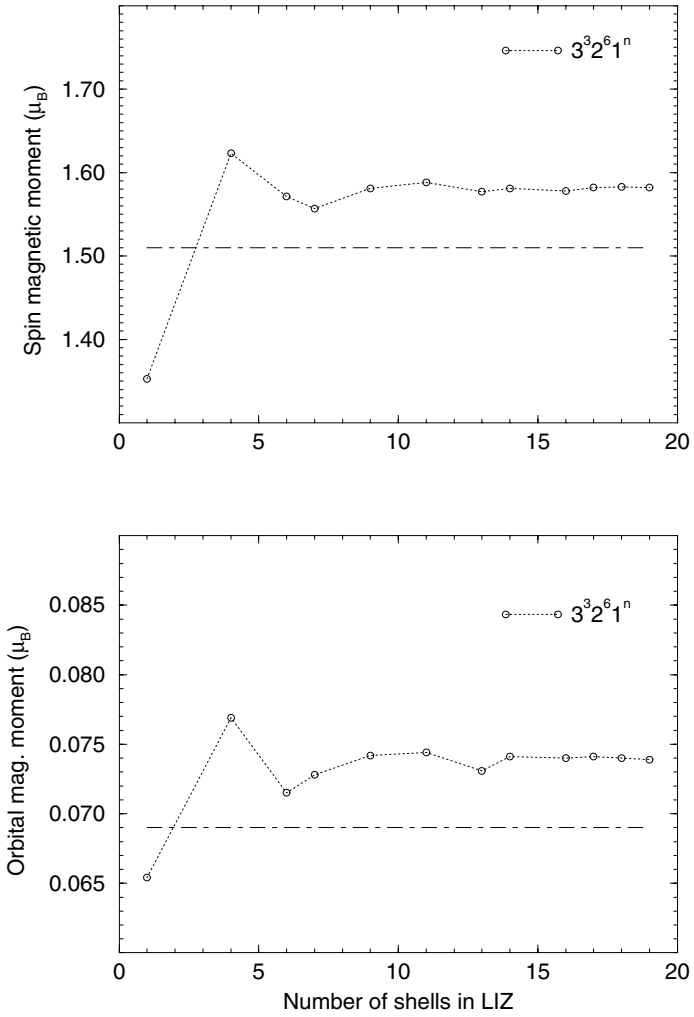

Figure 3. Convergence of the spin and orbital magnetic moments of fcc Co as a function of shells in the LIZ. The angular momentum configuration used is $l_{max} = 3^3 2^6 1^n$ (dotted line). The screening radius consists of one shell. The dashed line corresponds to the KKR $\boldsymbol{k}$-space result [24].

the moments showed no sign of convergence even for seven shells in the LIZ. Larger cluster sizes could not be investigated with the unscreened real-space code, as the CPU times became prohibitive. With the screened version of the method one can explore much larger cluster sizes, and we find that the magnetic moments only start to converge for LIZs containing more than 1200 atoms, i.e., at least 32 shells. For the LIZ of 1253 atoms (33 shells, $l_{max} = 3^3 2^6 0^{25}$), we find the converged value of the spin magnetic moment to be 0.598 μ_B. Note that in our calculations, $l_{max} = 3$ has been implemented only on the central site and the two surrounding shells. Including also the $l = 3$ contributions from further shells changes the moments on the central site only marginally. Equivalently, the inclusion of the $l = 1$ scattering channel from all the sites in the LIZ leads only to minor changes in the moments, which is why the $l = 1$ contributions beyond the eight shells are ignored in the case of Ni, where we have to investigate very large cluster sizes. The fact that the $l = 3$ and $l = 1$ contributions do not

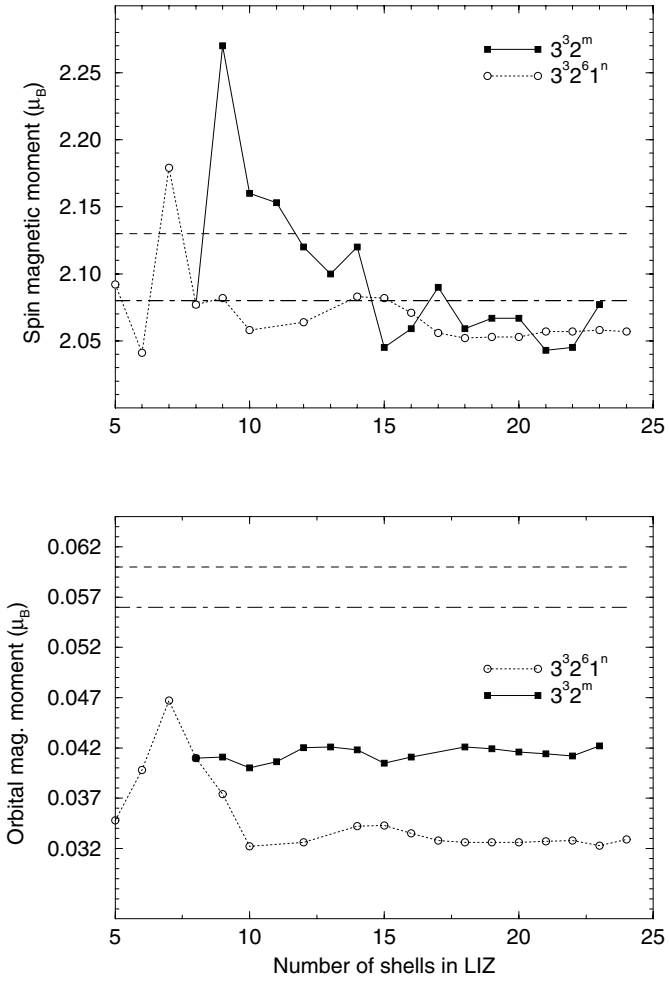

Figure 4. Convergence of the spin and orbital magnetic moments of bcc Fe as a function of the number of shells in the LIZ. The angular momentum configurations used are $l_{max} = 3^3 2^6 1^n$ (dotted line) and $l_{max} = 3^3 2^m$ (solid line). A screening radius of two shells is used. The dashed and dashed–dotted lines correspond to the KKR $\boldsymbol{k}$-space results given by Strange *et al* [25] and Ebert *et al* [24].

significantly influence the convergence of the magnetic moments might, in the tight-binding picture, be understood as being related to the fact that f or p electrons of these constituent atoms hardly contribute to the valence band on the central site.

The execution times of the self-consistency cycles increase significantly as a function of the number of sites with $l_{max} = 2$. Therefore in the case of Ni for example, when going beyond the eighth shell, both the $l = 2$ and $l = 1$ scattering channels are no longer included, which means that in the present approximation (dotted line in figure 5), the p, d and f contributions from sites beyond the central area have been removed. The substantial long-range effects that we see in Ni, implying that the multiple scattering from sites situated on shells far away still influences the electronic structure on the central site, seem to originate from the s scattering channel. Similarly for Fe and Co, those sites situated beyond the eighth shell are assumed to contribute only to the s and p scattering.

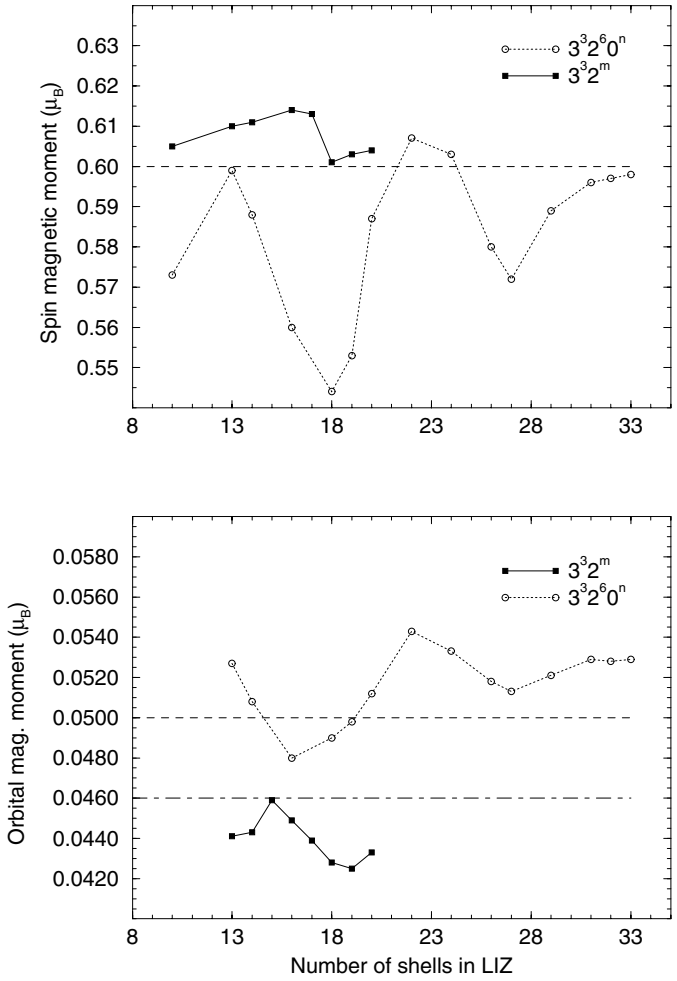

Figure 5. Convergence of the spin and orbital magnetic moments of fcc Ni as a function of the number of shells in the LIZ. The angular momentum configurations used are $l_{max} = 3^3 2^6 0^n$ (dotted line) and $l_{max} = 3^3 2^m$ (solid line). A screening radius of one shell is used. The dashed and dashed–dotted lines correspond to the KKR $\boldsymbol{k}$-space results given by Strange *et al* [25] and Ebert *et al* [24].

In the tight-binding picture, the $l = 2$ contributions are due to the overlap of the atomic d levels. The solid line in figure 4 shows the convergence of the magnetic moment of Fe, and for the angular momentum configurations $l_{max} = 3^3 2^m$, i.e. the $l = 2$ contribution from all the sites in the LIZ are taken into account here. It can be seen that, although there are considerable differences for small LIZs, the converged value seems less dependent on whether the $l = 2$ scattering channel is included. This implies that it is mainly the itinerant s contribution, through s–d hybridization, that determines the magnetic moment on the central site of the LIZ. As expected, the orbital moment is more sensitive to the angular momentum convergence. In particular, we note from figure 4 a 20% variation in the orbital moment between the angular momentum configuration $l_{max} = 3^3 2^m$ and $l_{max} = 3^3 2^6 1^n$.

A similar picture emerges for Ni (figure 5), although we have not been able to investigate the convergence for LIZs larger than 19 shells, i.e. $l_{max} = 3^3 2^{17}$. The results seem to

indicate that the converged magnetic moment will not differ considerably from the value obtained with the configuration $l_{max} = 3^3 2^6 0^{25}$. The values for the spin and orbital magnetic moments that are given in table 1 correspond to the largest possible LIZ that we were able to investigate, i.e. 1253 atoms with the angular momentum configurations $l_{max} = 3^3 2^{15} 0^{16}$ and $l_{max} = 3^3 2^{11} 0^{16}$ for respectively one and two shells of screening. For small LIZs, as can be seen from figure 5, the variation in the magnetic moment is much less pronounced. This might be due to the fact that for close-packed fcc Ni the d contributions are screened out faster than in the more open bcc structure (compare to the result for Fe). Thus, the angular momentum cut-off, justified for p and f contributions, needs to be employed with care when dealing with the d contributions.

Table 1. Screened real-space results for the spin and orbital moment of Fe, Co and Ni, compared to corresponding results obtained by the $\boldsymbol{k}$-space KKR method and the unscreened LSMS method.

	Fe (bcc)		Co (fcc)		Ni (fcc)	
Method	$\boldsymbol{m}_s(\mu_B)$	$\boldsymbol{m}_o(\mu_B)$	$\boldsymbol{m}_s(\mu_B)$	$\boldsymbol{m}_o(\mu_B)$	$\boldsymbol{m}_s(\mu_B)$	$\boldsymbol{m}_o(\mu_B)$
This work						
Two-shell screened (LIZ = 609 atoms)	2.057	0.033				
Three-shell screened (LIZ = 531 atoms)	2.109	0.035				
One-shell screened (LIZ = 555 atoms)			1.58	0.074		
One-shell screened (LIZ = 1253 atoms)					0.62	0.044
Two-shell screened (LIZ = 1253 atoms)					0.60	0.045
SPR-LSMS [7]						
(LIZ = 65 atoms)	2.08	0.041				
(LIZ = 87 atoms)			1.59	0.074		
(LIZ = 135 atoms)					0.546	0.044
KKR [23]	2.15		1.56		0.59	
SPRKKR [24]	2.08	0.056	1.51	0.069	0.60	0.046
SPRKKR [25]	2.13	0.06			0.60	0.05
Experiment [22]	2.13	0.09			0.57	0.05

4.2. Real space versus $\boldsymbol{k}$-space

In the limit of the 'exact' real-space implementation, i.e. for large screening radii and large LIZs, our results should converge to the 'exact' $\boldsymbol{k}$-space KKR results. In table 1, we compare our results for the spin and orbital magnetic moments to the experiment [22] and results obtained with the unscreened real-space method and the $\boldsymbol{k}$-space techniques [23–25]. The results given by Moruzzi *et al* [23] are non-relativistic, which explains why there is no value for the orbital moment. The first fully relativistic KKR calculations, with spin polarization and spin–orbit coupling being treated on an equal footing, are those given by Ebert *et al* [24] and Strange *et al* [25], marked respectively by the dashed–dotted and dashed lines in figures 4 and 5.

For Fe, we see that we have very good agreement for the spin magnetic moment with both the $\boldsymbol{k}$-space KKR method and the experiment. For the orbital moment of Fe the agreement is not as satisfactory as for the spin moment. However, the orbital moment is not well reproduced by any band-structure method, except maybe for the calculation by Trygg *et al* [26], who used the full-potential LMTO, both with and without orbital polarization (OP), finding a much improved agreement with experiment when the orbital polarization has been taken into account. The spin moments are insensitive to whether OP is included or not. This may

indicate the importance of going beyond the local spin density (LSD) and considering the effect of orbital currents.

The screened real-space results for Ni were obtained by using a LIZ of 1253 atoms (33 shells) and the respective angular momentum configurations were $l_{max} = 3^3 2^{11} 0^{20}$ with two shells of screening and $l_{max} = 3^3 2^{15} 0^{16}$ with one shell of screening. Again the agreement with the $\boldsymbol{k}$-space methods has been very good, in particular as regards the value for the orbital moment. These results show that our real-space approach has converged for the magnetic moment within the accuracy of the present state-of-the-art calculations. The spin magnetic moment is in general a more robust quantity to converge whilst the orbital magnetic moment is sensitive to the angular momentum cut-off in real space.

4.3. Magnetocrystalline anisotropy energy

In table 2, we compare our results for the magnetocrystalline anisotropy energy for the transition metals, as a function of the LIZ size and screening radius, to the results of the $\boldsymbol{k}$-space methods [27, 28]. For the bulk, these energies are extremely small, i.e. of the order of μeV. Therefore, to get meaningful results, the band energies had to be converged to the accuracy of at least 10^{-8} eV. To accomplish this, up to a hundred iterations in the self-consistency cycle have been needed for the modest sizes of the LIZs and screening radii. Note that the $\boldsymbol{k}$-space methods, which we compare our results to, also suffer due to the latter and additionally have problems with the Brillouin zone integrations, where huge numbers of $\boldsymbol{k}$-points are needed to determine the tiny MAEs. Here the MAE is calculated as the one-electron sum energy difference for the magnetizations pointing along the [001] and [111] directions, i.e. $\mathrm{MAE} = E_{sum}^{[001]} - E_{sum}^{[111]}$.

Table 2. Results for the magnetocrystalline anisotropy energy, $E_{sum}^{[001]} - E_{sum}^{[111]}$, for fcc Co, fcc Ni and bcc Fe. The screened real-space method results are compared to the unscreened real-space method and the $\boldsymbol{k}$-space method.

Method	MAE (μeV/atom) fcc Co	MAE (μeV/atom) fcc Ni	MAE (μeV/atom) bcc Fe
This work			
One-shell screened (LIZ = 555 atoms)	0.544		
One-shell screened (LIZ = 135 atoms)		1.8	
One-shell screened (LIZ = 1175 atoms)		2.2	
Two-shell screened (LIZ = 135 atoms)		−0.31	
Two-shell screened (LIZ = 1175 atoms)		−0.34	
Two-shell screened (LIZ = 65 atoms)			−0.73
Two-shell screened (LIZ = 339 atoms)			−0.66
SPR-LSMS [7]			
(LIZ = 87 atoms)	1.050		
(LIZ = 135 atoms)		−0.434	
(LIZ = 65 atoms)			−0.78
SPRKKR [27]		10.5 ± 7.0	
SPRKKR [28]	0.86	0.11	−0.95
Experiment [22]	1.52	2.7	−1.3

For Co and Fe, the correct easy axis of the magnetization is found, i.e., the sign agrees with the one observed experimentally. When compared to experiment, our values for the MAE are too small by a factor of 3 for Co and a factor of 2 for Fe, but fit well within the rather broad

range of values found by $\boldsymbol{k}$-space KKR and LMTO [26] calculations. Our results are smaller than the corresponding KKR $\boldsymbol{k}$-space values and the unscreened real-space values. The reason for this is most probably insufficient convergence with respect to the screening radius.

For Ni, we find the wrong easy axis of magnetization. This result is in agreement with the LMTO calculations [26,29,30], whereas Razee *et al* [28], using the $\boldsymbol{k}$-space KKR method, have obtained a positive value. In Ni, d electrons are slightly more localized, which is indicated by a narrower d band, and one may expect the orbital moment to play a more prominent role in this system. Trygg *et al* [26] have taken this into account by including the orbital polarization effects within the full-potential LMTO method (FP-LMTO-OP). Whereas this usually gives a better agreement with experimental results as regards the magnitude, it does not have any effect on the sign of the magnetic anisotropy, i.e., they also find the wrong easy axis for Ni. In their calculations the MAE has been obtained from the total energies, i.e., the force theorem has not been used. Since the LSD has been the only approximation used in their calculation, one is inclined to conclude that the LSD cannot describe Ni, because the orbital motion of the electrons cannot be well represented by the free-electron gas [31].

Further to our results, we should mention that although the MAE is rather insensitive to the size of the LIZ, it is very dependent on the size of the screening radius, which needs to be large enough for good convergence. Also, as can be seen in table 2, the sign of the magnetic anisotropy energy of Ni can change when a screening radius of two shells is used instead of the screening radius of only one shell.

What we have not been able to investigate in this paper with respect to the MAE, because of the huge matrix sizes it gives rise to, is the influence of the angular momentum cut-off, when going beyond the eighth shell in the LIZ. We have seen that the magnetic moment has been very sensitive to this, and it would have been interesting to see the effect, if any, on the MAE. Since it is possible to approximately determine the MAE using relatively small clusters, it seems that one is dealing here with a phenomenon that is rather localized in space. Overall, our results have been quite satisfactory, indicating that within the validity of the LSD, the MAE can be calculated in real space to an acceptable degree of accuracy.

4.4. Orbital moment anisotropy

In transition metals, both the MAE and the orbital moment are due to the spin–orbit coupling [32]. It has been shown by Bruno [33], when treating the spin–orbit interaction in first-order perturbation theory and assuming the band splitting to be much larger than the crystal-field splitting, that the magnetocrystalline anisotropy energy, with respect to the magnetization directions $\hat{M}_1$ and $\hat{M}_2$, is related to the corresponding anisotropy in the orbital moment through

$$E_{sum}^{[\hat{M}_1]} - E_{sum}^{[\hat{M}_2]} = \frac{\xi}{4\mu_B}(m_{orb}^{[\hat{M}_2]} - m_{orb}^{[\hat{M}_1]}) \tag{8}$$

where ξ is the spin–orbit coupling parameter. From this equation it follows that it should be possible to identify the easy axis from the magnetization direction which has the largest orbital moment [3,4]. If the magnetization lies along the hard axis, the spin–orbit coupling will force the orbital moment away from its preferred direction, giving rise to a small component of the orbital moment along the hard axis.

For all systems studied, we have calculated the components of the orbital moment for the magnetization along both the [001] and the [111] directions. Defining the anisotropy in the orbital moment as OMA $= L_z^{[001]} - L_z^{[111]}$, we have found for Co and Ni, respectively, the values of $-52 \times 10^{-6}\ \mu_B$ and $78 \times 10^{-6}\ \mu_B$. Since for the fcc structure the easy axis is along the [111] direction, one can see that our real-space calculations (based on formula (8))

give the wrong easy axis of magnetization for Ni, but the correct easy axis is obtained for Co, where the orbital moment is largest for the magnetization along [111].

The value of the orbital moment is very sensitive to the assumed angular momentum configuration in the LIZ. It has been noticed in the case of the bcc Fe that the LIZs of the same size, but with a different number of shells with the $l_{max} = 2$ configuration on the sites, can actually lead to different signs for the OMA. Namely, for the LIZ of 339 atoms, and the angular momentum configurations of respectively $l_{max} = 3^3 2^6 0^8$ and $l_{max} = 3^3 2^7 0^7$, we have calculated the OMAs to be $-2.98 \times 10^{-6}\ \mu_B$ and $28 \times 10^{-6}\ \mu_B$ whilst the sign of the MAE remains unaltered. The force theorem has been used to derive both the MAEs and the OMAs. Although there is no proof for the variational nature of the OMA, it has been reassuring that a fully self-consistent calculation for both magnetization directions for the $l_{max} = 3^3 2^6 0^8$ configuration has also given OMA $= -2.98 \times 10^{-6}\ \mu_B$, thus justifying the use of the force theorem.

The easy axis for bcc Fe is along [001], and our results show that to get the correct easy axis, the $l = 2$ contributions are of paramount importance. Thus, the MAE is less sensitive to the $l = 2$ contributions than the OMA, which might be due to the fact that the orbital moment points along a specific direction and its calculation requires a higher angular momentum expansion. Note also that for 65 atoms in the LIZ, and with all the sites having at least $l_{max} = 2$, the OMA is $17.3 \times 10^{-6}\ \mu_B$, i.e. it has the correct sign. The actual angular momentum configuration for this cluster is $l_{max} = 3^3 2^3$, i.e. there are fewer shells with $l_{max} = 2$ than in either of the two configurations for the cluster of 339 atoms, discussed above. What these results seem to imply is that as long as the convergence with respect to the $l = 2$ contributions has not been reached, including as many outer shells as possible with the $l_{max} = 0$ configuration gives worse accuracy than when simply restricting the size of the LIZ cluster, but having the $l_{max} = 2$ configuration on all the sites.

5. Conclusions

We have shown that the screened relativistic and spin-polarized real-space KKR band-structure method can be useful for studying magnetic properties of solids. Owing to the exponentially decaying screened structure constants and the use of the sparse matrix techniques, the inversion of the corresponding KKR matrix scales nearly as $O(N)$. The subsequent gains in the execution times allow one to study systems with local interaction zones of more than a thousand atoms. However, it is important to find the right balance between the size of the LIZ and the angular momentum configuration. The magnetic moments on the central site can be obtained to a good accuracy with restricted angular momentum configurations, but may need substantial LIZs as we demonstrated for Ni. On the other hand, directional properties, such as the MAE and the OMA, require the inclusion of the $l_{max} = 2$ configuration on all the sites of the LIZ. In this case the size of the LIZ is not so much the determining quantity. Of course, a drawback of the method is that the screened structure constants need to be calculated numerically. Since the dimension of the screened structure constant matrix and its sparsity are the determining factors in the matrix inversion, approximations with respect to the screening radius and the on-site angular momentum configuration have to be implemented. Their implications have been thoroughly examined, and it has been found out that the d scattering channel has been most sensitive to those approximations. The present application to the elemental transition metals, the fcc Co and Ni, and the bcc Fe, to study their magnetic properties, has been motivated by the need for benchmarking the method. While the spin and orbital magnetic moments of Fe and Co have turned out to converge fast in real space, the LIZs of about 1200 atoms have been necessary to reach convergence for Ni. It has been encouraging, however, that the converged values for

these quantities compare well with the results of the corresponding $\boldsymbol{k}$-space methods. The fact that we have succeeded in calculating the magnetic moments and the magnetocrystalline anisotropy energies within a real-space approach proves that these properties are determined by the local environment, and that the method can provide new insight into the physics at the origin of magnetism in these materials. Unfortunately, the computational effort, for very large LIZs, can be quite substantial. The specific two-shell screening result for Ni in table 1 took a week to complete on a 500 MHz DEC-Alpha workstation, whereas the same result could be easily obtained in minutes with the $\boldsymbol{k}$-space KKR. However, it is not the elemental transition metals that the method is aimed at. For periodic systems, where $\boldsymbol{k}$-space methods can be applied, the present real-space method is uncompetitive, but not many real systems are periodic. At interfaces and grain boundaries, for steps on surfaces and for nanowires, for example, the $\boldsymbol{k}$-space methods can no longer be applied, and it is here that the advantage of the present method can be appreciated and moreover can be implemented with varying degrees of accuracy depending on the amount of computational effort one wishes to use.

Acknowledgments

Useful discussions with Professor Peter H Dederichs and Dr Rudi Zeller are highly appreciated. Moreover, one of us (LP) would like to acknowledge the financial support of the Psi-k European Network, and the TMR 'Interface Magnetism' Network (contract FMRX-CT96-0089).

References

[1] Berkowitz A E, Mitchell J R, Carey M J, Young A P, Zhang S, Spada F E, Parker F T, Hutten A and Thomas G 1992 *Phys. Rev. Lett.* **68** 3745
[2] Xiao J Q, Jiang J S and Chien C L 1992 *Phys. Rev. Lett.* **68** 3749
[3] Dürr H A, Guo G Y, van der Laan G, Lee J, Lauhoff J A C and Bland J A C 1997 *Science* **277** 213
[4] Hjortstam, O, Baberschke, K, Wills J M, Johansson B and Eriksson O 1997 *Phys. Rev.* B **55** 15 026
[5] Nicholson D M C, Stocks G M, Wang Y, Shelton W A, Szotek Z and Temmerman W M 1994 *Phys. Rev.* B **50** 14 686
[6] Wang Y, Stocks G M, Shelton W A, Nicholson D M C, Szotek Z and Temmerman W M 1995 *Phys. Rev. Lett.* **75** 2867
[7] Beiden S V, Temmerman W M, Szotek Z, Gehring G A, Stocks G M, Wang Yang, Nicholson D M C, Shelton W A and Ebert H 1998 *Phys. Rev.* B **57** 14 247
[8] Beiden S V, Guo G Y, Temmerman W M, Szotek Z, Gehring G A, Wang Y, Stocks G M, Nicholson D M C, Shelton W and Ebert H 1996 *Materials Theory, Simulations and Parallel Algorithms (MRS Proc. No 408)* ed E Kaxiras, J Joannopoulos, P Vashishta and R K Kalia (Pittsburgh, PA: Materials Research Society)
[9] Braspenning B J and Lodder A 1994 *Phys. Rev.* B **49** 10 222
[10] Andersen O K and Jepsen O 1984 *Phys. Rev. Lett.* **53** 2571
[11] Andersen O K, Postnikov A V and Savrasov S Y 1992 *Application of Multiple Scattering Theory to Materials Science (MRS Proc. No 253)* ed W H Butler, P H Dederichs, A Gonis and R L Weaver (Pittsburgh, PA: Materials Research Society)
[12] Zeller R, Dederichs P H, Ujfalussy B, Szunyogh L and Weinberger P 1995 *Phys. Rev.* B **52** 8807
[13] Petit L, Beiden S V, Temmerman W M, Szotek Z, Stocks G M and Gehring G A 1998 *Phil. Mag.* B **78** 449
[14] Zeller R 1997 *Phys. Rev.* B **55** 9400
[15] Szunyogh L, Ujfalussy B, Weinberger P and Kollar J 1994 *Phys. Rev.* B **49** 2721
[16] Wildberger K, Zeller R and Dederichs P H 1997 *Phys. Rev.* B **55** 10 074
[17] Duff I S 1996 *Rutherford Appleton Laboratory Report No* RAL-TR-047
[18] Strange P, Ebert H, Staunton J B and Gyorffy B L 1989 *J. Phys.: Condens. Matter* **1** 2959
[19] Strange P, Staunton J and Gyorffy B L 1984 *J. Phys. C: Solid State Phys.* **17** 3355
[20] Mackintosh A R and Andersen O K 1980 *Electrons at the Fermi Surface* ed M Springford (Cambridge: Cambridge University Press)
[21] Zeller R, private communication
[22] *Landolt–Börnstein New Series* 1988 Group III, vol 19a, ed H P J Wein (Berlin: Springer)

[23] Moruzzi V L, Janak J F and Williams A R 1978 *Calculated Electronic Properties of Metals* (New York: Pergamon)
[24] Ebert H, Strange P and Gyorffy B L 1988 *J. Phys. F: Met. Phys.* **18** L135
[25] Strange P, Staunton J B, Gyorffy B L and Ebert H 1991 *Physica* B **172** 51
[26] Trygg J, Johansson B, Eriksson O and Wills J M 1995 *Phys. Rev. Lett.* **75** 2871
[27] Strange P, Ebert H, Staunton J B and Gyorffy B L 1989 *J. Phys.: Condens. Matter* **1** 3947
[28] Razee S S A, Staunton J B and Pinski F J 1997 *Phys. Rev.* B **56** 8082
[29] Daalderop G H O, Kelly P J and Schuurmans M F H 1990 *Phys. Rev.* B **41** 11 919
[30] Guo G Y, Temmerman W M and Ebert H 1991 *Physica* B **172** 61
[31] Jansen H J F 1995 *Phys. Today* (4) 50
[32] Brooks H 1940 *Phys. Rev.* **58** 909
[33] Bruno P 1989 *Phys. Rev.* B **39** 865